

LETTER TO THE EDITOR

The neutral gas phase nearest to supermassive black holes

A massive neutral-atom- and molecule-rich broad line region in active galactic nuclei

Thi W.-F.¹ and Papadopoulos, P. P.^{2,3,4}

¹ Max Planck Institute for Extraterrestrial Physics, Giessenbachstrasse, 85741 Garching, Germany e-mail: wingfai.thi@googlemail.com

² Department of Physics, Section of Astrophysics, Astronomy and Mechanics, Aristotle University of Thessaloniki, GR-54124 Thessaloniki, Greece e-mail: padelis@auth.gr

³ Research Center for Astronomy, Academy of Athens, Soranou Efessiou 4, GR-11527 Athens, Greece

⁴ School of Physics and Astronomy, Cardiff University, Queens Buildings, The Parade, Cardiff CF24 3AA, UK

... ; ...

ABSTRACT

Context. Broad line regions (BLRs) are known to contain gravitationally bound gas within a $r \sim (\text{few}) \times (10^2 - 10^3)$ Schwarzschild radii (R_S) near supermassive black holes (SMBHs) in active galactic nuclei (AGNs). Photo-ionized by a strong non-stellar AGN continuum, this gas emits luminous ultraviolet/optical/near-infrared lines from ionized hydrogen (and other multi-ionized atoms) that have the widest velocity profiles observed in galaxies, uniquely indicating the deep gravitational wells of SMBHs.

Aims. Nearly all BLR studies focus on its ionized gas phase (hereafter BLR⁺), with typical masses of only $\sim (\text{few}) \times (10 - 100) M_\odot$, despite strong indications of neutral BLR gas reservoirs (hereafter, BLR⁰) with $M_{\text{BLR}^0} \sim 10^{5-6} M_\odot$.

Methods. We used the photoionization code CLOUDY, with its chemistry augmented using three-body reactions, to explore 1D models of dustless BLRs, focusing on the BLR⁰ conditions and the abundances of its most prevalent neutral atoms and molecules.

Results. A (neutral-atom-) and molecule-rich BLR⁰ gas phase is found to be underlying the BLR⁺. The latter occupies only a thin outer layer of AGN-irradiated gas column densities, while the former contains the bulk of the BLR gas mass. Atomic carbon and oxygen as well as the CO molecule can reach substantial abundances in the BLR⁰, while their lines at infrared (IR) and submillimeter (submm) wavelengths can yield new probes of the BLR physical conditions and dynamics, unhindered by the dust absorption from outer AGN tori that readily absorb the BLR⁺ optical and far-ultraviolet (FUV) lines.

Conclusions. We find that neutral-atom-rich and even molecule-rich gas can exist in the BLR⁰. The corresponding spectral lines from neutral atoms and molecules promise a new spectral window of gas dynamics in the vicinity of SMBHs unhindered by dust absorption. This may even offer the prospect of conducting novel tests of general relativity in strongly curved spacetime.

Key words. galaxies: active – quasars: emission lines – ISM: molecules – ISM: atoms – quasars: general – AGN: BLR

1. Introduction

The probability of a neutral-atomic or even molecule-rich gas phase having any significant mass lying in the vicinity ($\sim (\text{few}) \times (10^2 - 10^3) R_S$, $R_S = 2GM_{\text{SMBH}}/c^2$) of a supermassive black holes (SMBH) in active galactic nuclei (AGNs) could be naively be considered as being virtually zero, given the extreme ultraviolet (UV) and hard X-ray non-stellar continua emanating from the SMBH accretion disks and their hot coronae, (e.g., Rokaki, Boisson, & Collin-Souffrin 1992; Thomas et al. 2016; Dewangan et al. 2021). The strong UV AGN continuum photoionizes such gas, sublimating its concomitant dust once its temperature rises above the sublimation limit of $T_{\text{dust}} \sim (1500 - 2000) \text{ K}$; this limit can be reached at distances of $r \leq R_{\text{sub}} \sim 0.2 [L_{\text{bol}} / (10^{46} \text{ erg s}^{-1})]^{1/2} \text{ pc}$ from the AGN (e.g., Baskin & Laor 2018). Photoionized gas seems an unlikely phase for the onset of a (neutral-atom and molecule)-rich chemistry; even a neutral but dustless gas phase would also seem to be as well, given the role of dust in catalysing H_2 formation (Gould & Salpeter 1963; Cazaux & Tielens 2002; Thi et al. 2020, and references therein).

Three important elements are missing from this simple picture, namely: a) a molecule-rich chemistry is possible even in hot dustless gas provided densities are high enough ($n_{\text{H}} \geq 10^{10} \text{ cm}^{-3}$); b) molecules such as H_2 or CO can strongly self-shield once formed even in initially small quantities; and c) the thermal (and thus chemical) gas properties are drastically altered once neutral atomic and/or molecular species form, even in initially low abundances because they are efficient gas coolants via their lines. Such a molecule-rich chemistry in hot, strongly UV-irradiated dense gas, whose concomitant dust reservoir is fully sublimated, has already been inferred in the disk around the B star 51 Oph (Thi et al. 2005, 2013). This result has subsequently been confirmed by spatially resolved near-infrared (NIR) interferometric observations of CO overtone lines (Tatulli et al. 2008; GRAVITY Collaboration 2021a). In addition, CO has even been detected in the X-ray-irradiated gas ejecta of SN 1987A Spyromilio et al. (1988), its formation mediated by He^+ charge-transfer reactions (Lepp, Dalgarno, & McCray 1990) in an environment that certainly ranks among the most hostile ones in the Universe with respect to a molecule-

rich chemistry.

The possibility of a neutral-atom- and molecule-rich gas phase in the vicinity of SMBHs, despite photoionization by a strong UV/X-ray AGN continuum, has been investigated in the past (Lepp et al. (1985)); however, these studies have not included the very important process of dust sublimation by the AGN radiation fields. This work was revisited by Kallman, Lepp, & Giovannoni (1987), which did not include H^- electron photo-detachment by IR radiation, another process that is fundamentally important for the chemistry in the strongly AGN-irradiated BLR gas. Ferland & Persson (1989), modeled the Ca II line triplet AGN observations, thereby correcting the two aforementioned omissions and arguing for the presence of a massive neutral BLR gas phase underlying the photo-ionized one. However these authors did not consider any neutral-atomic or molecular abundances past the BLR^+/BLR^0 boundary¹, reporting $N(H)_{\min,0} \sim 10^{24.5} \text{ cm}^{-2}$ as the minimum column density necessary for explaining the Ca II triplet IR-line strengths relative to its UV lines and other lines emanating from the BLR^+ . Nevertheless, the very same arguments presented by Ferland & Persson (1989), along with the obvious expectation that neutral-atoms and molecules will form at the deeper end of any 1-side irradiated BLR gas column densities, (e.g., Gaskell 2009), as well as general arguments made throughout the AGN literature about an underlying BLR^0 being much more massive than the BLR^+ , (e.g., Baldwin et al. 2003; Ferland 2004), all require any new state-of-the-art BLR models to extend well past the aforementioned minimum gas column density.

In this work, we examine the thermal state and the abundances of a few key atomic and molecular species in a dust-less BLR^0 , for gas columns up to $\sim(\text{few}) \times 10^{26} \text{ cm}^{-2}$, and a typical AGN SED and radiation field strength. We then briefly comment on the possible use of neutral-atom and/or molecular line emission at IR and submillimeter (submm) wavelengths as extinction-free probes of the bulk of the BLR mass and the gas velocity fields near SMBHs. It may even be useful for carrying out novel tests of general relativity (GR) near SMBHs, as recently proposed by Kostaros, Papadopoulos, & Pappas (2024).

2. The CLOUDY code

We utilized the CLOUDY 23.01 (Gunasekera et al. 2023) photoionization and photodissociation code with the standard AGN-input spectral energy distribution (SED). CLOUDY includes photodissociation region (PDR) physics and has been benchmarked against other (PDR) codes (Röllig et al. 2007). We adopted a one-sided illuminated plan-parallel geometry. The chemical network is based on the UMIST 2012 Database for Astrochemistry, with enhanced metal abundance ($Z/Z_\odot = 5$) and specific extensions of the chemical rates (Shaw et al. 2022); these are especially relevant for chemical reaction rates at $T_{\text{gas}} \geq 100 \text{ K}$ (Shaw et al. 2023). Reactions relevant to PDR modeling are present in the CLOUDY network, including reactions with excited H_2 . The default network has been complemented by relevant three-body and calcium reactions (see Appendices A and C). The relative abundances follow the default ISM values. No grains nor PAHs are present because their temperature would be higher than their sublimation temperature in most part of the BLR, although the gas and dust temperature can

be below the dust sublimation limit at very high column densities. The potential effects of any remaining dust grains in the BLR will be further explored in a forthcoming paper. In the absence of dust grains, H_2 , C, and CO can only self-shield and self each other against photodissociation (Hollenbach & Tielens 1999). The cosmic-ray flux density was set to the default value.

3. The BLR^0 vs the BLR^+ : Model parameters

Ever since their discovery (Seyfert 1943), the luminous and very broad ($FWZI \sim (10^3 - 10^4) \text{ km s}^{-1}$) lines of the BLR^+ at UV/optical/NIR wavelengths have been AGN signposts, revealing the deep gravitational potential of SMBHs within $\sim(500-10^4) R_S$. Powered by photoionization from a strong non-stellar AGN continuum that yields ionized hydrogen (and other multiply ionized atoms), these lines are used to study the BLR conditions (e.g., density, ionization, temperature, and metallicity Netzer 1990; Korista & Goad 2004; Peterson 2006; Gaskell 2009). However the sharpness of the H^+/H transition zone with

$$\frac{\Delta R}{R_+} \sim 3.5 \times 10^{-4} \left[\left(\frac{S_{\text{ion}}}{10^{49} \text{ s}^{-1}} \right) \left(\frac{n}{100 \text{ cm}^{-3}} \right) \right]^{-1/3} \quad (1)$$

giving the width ΔR of this zone (assuming a Strömgren sphere of photoionized gas of radius, R_+ , with S_{ion} as the ionizing source's photoionization rate). This renders the BLR^+ main lines (i.e., the H recombination lines) incapable of probing the BLR^0 and, thus, of the total ($BLR^0 + BLR^+$) gas mass as well. For instance, this gives $n_H = 10^{11} \text{ cm}^{-3}$: $\Delta R/R_+ \sim 7.5 \times 10^{-7} [S_{\text{ion}}/(10^{49} \text{ s}^{-1})]^{-1/3} \ll 1$ for typical S_{ion} rates for AGNs. Lines from ionized and neutral atoms with ionization potentials lower than that of H (e.g., Fe^+ , Ca^+ , C, and O) is able probe the neutral gas past the H^+/H transition zone, yet deeper within, some can be locked into molecules, even in the absence of dust.

This leaves two key aspects open for inquiry: a) the actual value BLR^0 gas mass and b) what lines are able to probe it in its entirety. We must first adopt plausible masses for the BLR^0 in order to set an $N(H)_{\text{max}}$ value in our 1-D CLOUDY models. This is a critical parameter since, for any given AGN radiation field and SED incident on a one-sided irradiated BLR gas layer, arbitrarily large BLR^0 columns can be obtained beyond the H^+/H transition zone, for a high enough $N(H)_{\text{max}}$ result. Direct BLR^+ gas mass estimates via hydrogen recombination lines give $M_{BLR^+} \sim (10-100) M_\odot$, while a set of necessarily more indirect arguments set the putative BLR^0 to be at least $M_{BLR^0} \sim (10^4-10^5) M_\odot$ (Baldwin et al. 2003; Gaskell 2009; Ferland 2004). On the other hand an $N(H)_{\min}$ value for BLR gas structures can be obtained by simply demanding the SMBH gravity dominates over the radiative pressure from the AGN radiation field (i.e., the BLR is gravitationally bound to the SMBH). This yields:

$$\langle N(H) \rangle > \frac{L_{\text{AGN}}}{4\pi G m_p c M_{\text{SMBH}}}, \quad (2)$$

namely: $N(H)_{\min} \sim (10^{23}-10^{24}) \text{ cm}^{-2}$ for typical SMBH masses, M_{SMBH} , and AGN luminosities, L_{AGN} . Furthermore, it is necessary for the so-called radiation-pressure-confined (RPC) ionization layers to be established within the BLR^+ s in a universal fashion (in pressure equilibrium with deeper neutral BLR gas layers) and to do so across eight orders of magnitude of AGN power (Baskin, Laor, & Stern 2014; Baskin & Laor 2018). Thus, this value must be $N(H) \geq 10^{24} \text{ cm}^{-2}$ (Baskin, Laor, & Stern 2014). This result is similar to the $N(H)_{\min} \sim 10^{24.5} \text{ cm}^{-2}$ value

¹ They made a comment only about H_2 (in their Appendix), which unlike Kallman, Lepp, & Giovannoni (1987), found it to be only a trace species, but otherwise giving no abundance estimates or profiles.

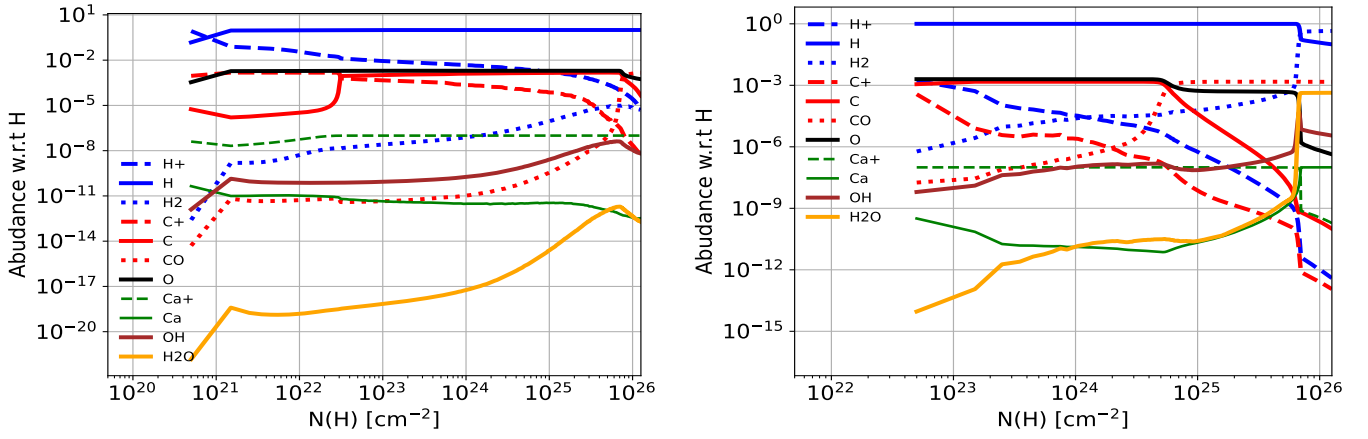


Fig. 1. Abundance for various species as function of the column density, *Left*: Model with $n_{\text{H}} = 10^{12} \text{ cm}^{-3}$, $\log(U) = -3$, and $\Delta V = 250 \text{ km s}^{-1}$, *Right*: Model with $n_{\text{H}} = 10^{14} \text{ cm}^{-3}$, $\log(U) = -5$, and $\Delta V = 250 \text{ km s}^{-1}$.

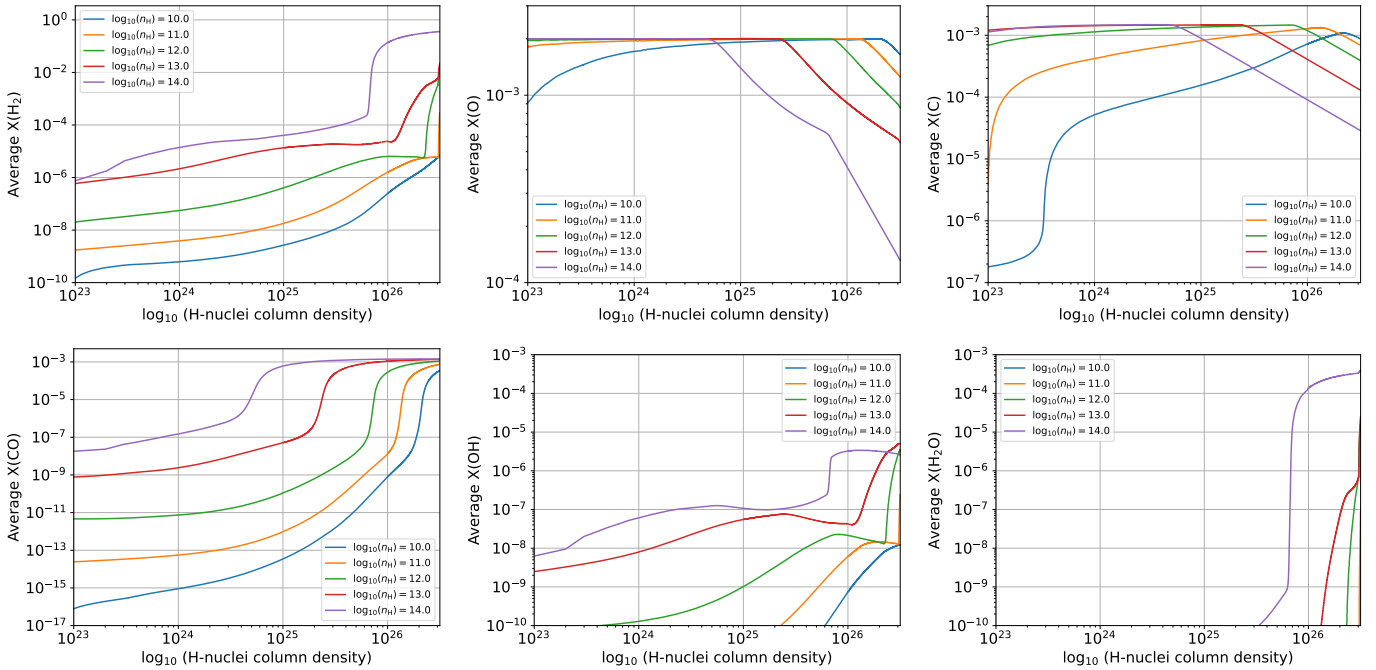


Fig. 2. Column density-averaged abundances for H_2 , O, C, CO, OH, and H_2O . The total H-column density varies slightly between models as the grid is determined by the code.

deduced from the Ca II triplet line observations, tracing low-ionization/neutral BLR gas layers (Ferland & Persson 1989). A maximum value for the total $N(\text{BLR}^+ + \text{BLR}^0)$ column density of the various BLR gas structures can then be simply set as: $N(\text{H})_{\text{max}} = N(\text{H})_{\text{BLR}^+} (1 + M_{\text{BLR}^0}/M_{\text{BLR}^+}) \sim N(\text{H})_{\text{min}} \times (10^2 - 10^4)$. For a $N(\text{H})_{\text{min}} = 10^{23} \text{ cm}^{-2}$, we adopted $\log_{10} N(\text{H})_{\text{max}} = 10^{26.5} \text{ cm}^{-2}$, with a $\log \Delta N(\text{H}) = 0.5$ grid step², and a BLR density range of $n_{\text{H}} = (10^{10}, 10^{11}, 10^{12}, 10^{13}, 10^{14}) \text{ cm}^{-3}$. For the ionization parameter, U , we adopted $U = 0.1$ for $n_{\text{H}} = 10^{10} \text{ cm}^{-3}$. The other U -grid values are chosen to make it so that the ionizing photon density, $n_{\gamma} = n_{\text{H}}U$, remains invariant; this is required by the AGN-induced dust sublimation condition holding within BLRs in all AGNs (Baskin, Laor, & Stern 2014). We considered the metallicities of $Z/Z_{\odot} = 5$, a super-solar value that is typical for BLR gas in galactic centers. Finally we adopt a

typical turbulent linewidth of $\Delta V = 250 \text{ km s}^{-1}$ for the BLR gas (Gaskell 2009)³. Fine physical grids were chosen to improve the model convergence. The temperature iteration tolerance was set to 5×10^{-3} (default value), while the grid parameters were: hydrogen density, n_{H} , ionization parameter, U , and the total hydrogen column density, N_{H} .

4. Results and discussion

Figure 1 shows the abundance of various species as function of $N(\text{H})$ for the $n_{\text{H}} = 10^{12} \text{ cm}^{-3}$, $\log(U) = -3$ model in the left panel and for the $n_{\text{H}} = 10^{14} \text{ cm}^{-3}$, $\log(U) = -5$ model in the right panel. From this figure, it is apparent that O and C are the two neutral atoms with the highest abundances dominating throughout the

³ This is an important parameter in any radiative transfer model as it regulates the escape probability of spectral line emission, gas cooling, and thus gas thermodynamics.

² The exact computed column density is set by the code.

BLR⁰ column, while deeper inside they react to form the dominant molecule expected in BLR⁰'s, namely, CO. The latter can reach up to a relative abundance $X(\text{CO}) \sim 10^{-4}$ – 10^{-3} deep inside that of BLR⁰, whereas H₂ remains only a trace element, as was already been established for dust-free BLRs by Ferland & Persson (1989) and Crosas & Weisheit (1993). This is quite unlike the ordinary ISM and, indeed, a CO-rich, yet H₂-poor gas phase is one of the peculiar hallmarks of a dust-free, but hot and very dense gas chemistry. Evidence for exactly such chemistry has already been uncovered for the hot, dust-free, inner gas disk around the B star 51 Oph Thi et al. (2005), with CO overtone lines even used to resolve the disk at sub-au scales GRAVITY Collaboration (2021a).

From Fig. 1, we see that for $n_{\text{H}} = 10^{12} \text{ cm}^{-3}$, the $\text{H}^+ \rightarrow \text{H}$ phase transition occurs at $N(\text{H}) \sim 10^{21} \text{ cm}^{-2}$, with neutral atomic H remaining dominant throughout the remaining BLR⁰ column. Only at the highest gas densities ($n_{\text{H}} = 10^{14} \text{ cm}^{-3}$) and largest BLR⁰ columns ($N(\text{H}) \sim 5 \times 10^{25} \text{ cm}^{-2}$) does the neutral atomic H becomes molecular (Fig. 1). Atomic oxygen, with its ionization potential (IP) of 13.618 eV only slightly above that of H (IP=13.598 eV), can remain neutral nearly throughout the H-rich BLR⁰ column. Atomic carbon on the other hand, with an IP of ~ 11.26 eV, can remain (singly) ionized inside the BLR⁰ past the $\text{H}^+ \rightarrow \text{H}$ transition, but by $N(\text{H}) \geq 3 \times 10^{22} \text{ cm}^{-3}$ (and $n_{\text{H}} = 10^{12} \text{ cm}^{-3}$), it becomes neutral. For higher densities though ($n_{\text{H}} = 10^{14} \text{ cm}^{-3}$) neutral atomic carbon dominates already from the BLR⁰ surface. Regarding CO, for $n_{\text{H}} = 10^{12} \text{ cm}^{-3}$, its abundance reaches $X(\text{CO}) \sim 10^{-4}$ only when $N(\text{H}) \geq 8 \times 10^{25} \text{ cm}^{-2}$ is reached; however, this transition happens in a much "shallower" segment within the BLR⁰ column, $N(\text{H}) \sim 6 \times 10^{24} \text{ cm}^{-2}$, at higher densities ($n_{\text{H}} = 10^{14} \text{ cm}^{-3}$).

It expected from the ionization potentials of Ca and Ca⁺ of IP=6.11 eV and 11.87 eV, respectively, that these two species are expected to be abundant in BLR⁰ (Ferland & Persson 1989). Figures 1 and C.1 show that the CaII abundance remains nearly constant across the entire BLR⁰ for $n_{\text{H}} = 10^{12} \text{ cm}^{-3}$, and it is only for the high-density model ($n = 10^{14} \text{ cm}^{-3}$) and large column densities ($\geq 6 \times 10^{25} \text{ cm}^{-2}$) that its abundance drops sharply due to e⁻ recombination into Ca; meanwhile, Ca-bearing molecules have very low abundances in all models. Only depletion onto dust grains has the ability to change the gas-phase elemental abundance of calcium, but this is not an option in dustless BLRs.

Figure 2 shows the $N(\text{H})$ -averaged abundances of H₂, O, C, CO, OH, and H₂O. The attenuation of the ionizing and molecule-dissociating radiation results in neutral and molecular species becoming abundant in BLR⁰. Nevertheless H₂ itself remains only a trace species, except at the highest densities as well as the highest column densities, where $X(\text{H}_2) \sim 0.1$ (Fig. 2, upper left). At high gas densities and temperatures up to ~ 1000 K: e⁻ recombination, neutral-neutral reactions with activation energy, and (potentially) three-body reactions are rapid because photoionization rates are $\propto n_{\text{H}}$, while recombination rates are $\propto n_{\text{H}}^2$. These reactions can overcome the (neutral-atom and molecule)-destructive reactions such as photoionization, collisional ionization, photodissociation, and the collisional molecular dissociation. The OH abundance is higher than that of H₂O in the $n_{\text{H}} = 10^{12} \text{ cm}^{-3}$ model, but it remains a secondary O-carrier; whereas for the highest density model ($n_{\text{H}} = 10^{14} \text{ cm}^{-3}$) and at $N(\text{H})$, water is the second most abundant oxygen carrier.

The chemical molecule-formation path in dense and hot gas starts with H₂ formation in the presence of sufficient C⁺, C, and O. In the absence of dust grains, H₂ is then formed solely via gas-phase reactions (Crosas & Weisheit 1993). Once formed, H₂ reacts with atomic oxygen to form OH, which in turn can re-

act with H₂ to form H₂O, or with singly ionized carbon to form CO via the reaction $\text{C}^+ + \text{OH} \rightarrow \text{CO}^+$, followed by $\text{CO}^+ + \text{H} \rightarrow \text{CO} + \text{H}^+$ (Elitzur 1979; Hollenbach & McKee 1989; Thi & Bik 2005). More details are given in Appendix F. Alternatively, OH can react with C to form directly CO at very high densities. In the absence of dust grains, atomic C, H₂, and CO molecules are shielded against photodissociation solely via line absorption, although the large intrinsic turbulence width significantly decreases the efficacy thereof. The CO/H₂ ratio is much higher than in the ordinary dusty molecular ISM, making CO the most abundant molecule and also making its lines potentially good BLR⁰ tracers. Furthermore, atomic oxygen, atomic carbon, OH, H₂O, and CO, once formed, act as very efficient gas coolants. This provides the capacity to strongly impact the gas thermal states, decreasing their temperature in deeper BLR⁰ layers. In principle this can push gas temperatures below the dust sublimation limit (~ 1000 – 1500 K, see Appendix E), allowing some dust to survive. Even trace amounts of dust surviving under BLR⁰ conditions can have a very strong impact on H₂ formation and to make the BLR⁰ very H₂-rich (Crosas & Weisheit (1993)). When very few dust grains survive in BLR⁰, the enhanced H₂ formation is due to the dust-enhanced attenuation of the molecule-dissociating AGN radiation field rather than to the classical H₂ formation route on dust grains. Indeed, even at $T_{\text{dust}} \sim 600$ K, the grains are still too warm to allow efficient formation of H₂ on their surfaces (Thi et al. 2020), while even a little dust can strongly attenuate the photodissociating far-UV flux, enhancing molecule formation. At the same time, gas-grain collisions, along with molecules, will cool the gas rapidly (especially at high gas densities), enhancing the conditions for a greater scale of molecule formation. Finally, H₂ can also form on PAHs (Boschman et al. 2015), which can survive in the hot environments of BLRs where silicate dust grains cannot. Thus inclusion of dust grains and PAHs in BLRs can further enhance the abundance of the molecular species such as H₂ and CO in their BLR⁰. Here, we must also note that for the inwards increasing gas density profiles expected in radiation pressure confined (RPC) BLR models (Baskin, Laor, & Stern 2014), the neutral atomic and molecular species abundances within BLR⁰'s can only be higher than those found for our uniform-density models.

Finally, for the strongly UV-deficient AGN SEDs associated with low $(dM/dt)/M_{\text{SMBH}}^2$ ratios (i.e., low accretion rates and/or hypermassive black holes, Laor & Davis 2011), their BLRs are expected to be even more neutral-atom- and molecule-rich, perhaps even completely lacking a BLR⁺ as an outside layer of the BLR⁰ (yielding the so-called "true" type 1 AGNs). These cases, along with the effects of small amounts of dust and PAHs and assuming a disk BLR configuration (as indicated by high-resolution BLR observations GRAVITY Collaboration (2018)) will be the subject of a forthcoming paper.

4.1. BLR⁰ lines: A new spectral window onto AGNs and extreme gas velocity fields near SMBHs

Atomic oxygen can emit a series of lines in the UV/optical/NIR and far-infrared (FIR) wavelength regimes (Bhatia & Kastner (1995) their Table 2). From these, we can see that only its two fine structure lines at $63.17 \mu\text{m}$ and $145.5 \mu\text{m}$ (due to $L \cdot S/r^3$ -type interaction term) can emanate from the BLR⁰, where the prevailing conditions are adequate for their collisions excitation up to full LTE levels. The rest of the O I lines, given the energy transitions between the (n, J) principal quantum numbers, are energetically too demanding to be collisionally excited within BLR⁰'s. Pumping by Ly β photons is necessary for the NIR O I

lines to be excited, placing them in the so-called low-ionization regions of the BLR⁺ (where such photons are readily available). Dias dos Santos et al. (2023) has recently detected a very wide, double peak, O I NIR line ($\lambda 11297$) in Zw 002 (Seyfert I), which may indeed be marking the low-ionization layer of a BLR⁺. The two fine structure lines of C I at ~ 492 GHz and ~ 809 GHz, along with the J -rotational lines of CO with $J=1-0$ (115 GHz) up to $J=6-5$, 7-6 (691 GHz, 806 GHz), are accessible through the Earth's atmosphere and will be LTE-excited in a BLR⁰. Deep ALMA observations; while, they cannot resolve C I and CO line emission in a BLR⁰, they are able to identify broad BLR⁰ lines provided that multi-tuned ALMA correlator setups are used to cover the $\sim(\text{few}) \times (10^3-10^4) \text{ km s}^{-1}$ velocity range. The highest- J CO lines accessible through the atmosphere (i.e., $J=6-5$, 6-7) are the best choices since for LTE-excitation: $\int_{\Delta\nu} S_{\nu}^{(\text{line})} d\nu \propto (J+1)^3 \nu_o^3 T_{\text{kin}}^4$ ($\nu_o \sim 115$ GHz). High-resolution ALMA observations of high- J CO lines of nearby AGNs do exist, (Gallimore et al. 2016), but their limited velocity coverage ($\sim 600 \text{ km s}^{-1}$), precludes them from identifying any ultra-wide BLR⁰ CO line emission. Warm CO-rich gas can emit ro-vibrational lines in the NIR-MIR that are then accessible to spatially resolved observations with IR interferometers, such as GRAVITY+ or MATISSE at ESO. GRAVITY has already been used in the past to identify dustless hot and dense CO-rich gas around 51 Oph. Although water can be abundant in the densest models, water lines are difficult to detect from ground-based telescopes and also require a favorable redshift.

4.2. Spectral line illumination of SMBHs: Possible new GR tests

Depending on their actual luminosities, the various neutral-atomic and/or molecular lines from the BLR⁰ gas disk can provide a novel spectral line, rather than a continuum, background illumination of the SMBHs in galactic centers. This aspect can enable new tests of Kerr versus non-Kerr Spacetimes around these ultra-relativistic objects, as recently proposed by Kostaros, Papadopoulos, & Pappas (2024).

5. Conclusions

Our work demonstrates the likely presence of neutral atoms and CO molecules in a potentially massive neutral gas BLR⁰ phase underlying the thin ionized layers of BLR⁺ in AGNs. In the dustless, albeit warm and dense, BLR⁰ gas, the prevailing molecule is CO; whereas H₂ remains only a trace species. The fine structure lines of neutral atomic oxygen and carbon at FIR and submm wavelengths can uniquely trace the BLR⁰ gas mass, while CO, with its rotational and ro-vibrational CO lines at mm/submm and NIR lines (also expected to be bright) open up a new observational spectral window to BLRs in AGNs and the extreme velocity fields near SMBHs. Gas density gradients, minute amounts of surviving dust (especially the thermally-resistant PAHs), and UV-photon deficient AGN SEDs (the result of low-accretion and/or hypermassive BHs in galactic centers) are all expected to further boost the abundances of neutral atoms and molecules in BLR⁰ and will be studied in detail in a forthcoming paper.

Acknowledgements. We would like to offer thanks to the referee, that helped us clarify some finer, yet important, points in the presented work. PPP would like

to acknowledge the hospitality of his colleague Wing-Fai Thi, in his apartment in Munich, where these ideas were developed.

References

- Baskin, A., Laor, A., & Stern, J. 2014, MNRAS, 438, 604
Baskin, A. & Laor, A. 2018, MNRAS, 472(2), 1970
Baldwin, A. J., Ferland, G.J., Korista, K.T., Hamann, F., & Dietrich, M. 2003, ApJ, 582, 590
Bhatia, A. K., & Kastner, S. O. 1995, ApJS, 96, 325
Boschman, L., Cazaux, S., Spaans, M., et al. 2015, A&A, 579, A72
Cazaux, S. & Tielens A. G. G. M. 2002, ApJ, 57, L29
Crosas, M. & Weisheit, J. C. 1993, MNRAS, 262, 359
Dewangan, G. C., Tripathi, P., Papadakis, I. E., & Singh K. P. 2021, MNRAS, 500, 1000
Dias dos Santos, D., Rodríguez-Ardila, A., Panda, S., et al. 2023, ApJ, 953, L3
Elitzur, M. 1979, ApJ, 229, 560
Elitzur, M. & Ho L. C. 2009, ApJ, 701, L91
Ferland, G., & Persson, S. E. 1989, ApJ, 347, 656
Ferland, G.: The broad emission line regions of quasars: Current status and future prospects. In: Richards, G.T., Hall, P.B. (eds.) AGN Physics with the Sloan Digital Sky Survey, vol. 311, p. 161. ASP Conference Series, San Francisco (2004)
Gallimore J., Elitzur M., Maiolino R., et al. 2016, ApJ, 829, L7
Gaskell, C.M.: What broad emission lines tell us about how active galactic nuclei work. New Astronomy Reviews 53(7-10), 140–148 (2009)
GRAVITY Collaboration: Sturm et al. 2018 Nature, 563, 657
GRAVITY Collaboration: Koutoulaki, M. et al. 2021, A&A, 645, 50
Gould, R. J., & Salpeter, E. E. 1963, ApJ, 138, 393
Gunasekera, C. M., van Hoof, P. A. M., Chatzikos, M., et al. 2023, Research Notes of the American Astronomical Society, 7, 246
Hollenbach, D. & McKee, C. F. 1989, ApJ, 342, 306
Hollenbach, D. J. & Tielens, A. G. G. M. 1999, Reviews of Modern Physics, 71, 173
Kallman, T., Lepp, S., & Giovannoni, P. 1987, ApJ, 321, 907
Korista, K. T., & Goad, M. R. 2004, ApJ, 606, 749
Kostaros, K., Papadopoulos, P., & Pappas, P. 2024 Phys. Rev. D Vol. 110, No. 2, 024001 – Published 2 July 2024
Laor, A., & Davies, S. W. 2011, MNRAS, 417, 681
Latter, W. B. & Black, J. H. 1991, ApJ, 372, 161
Lepp, S., McCray, R., Shull, M., Woods, D. T., & Kallman, T. 1985, ApJ, 288, 58
Lepp, S., Dalgarno, A. & McCray, R. 1990, ApJ, 358, 262
McElroy D., Walsh C., Markwick A. J., Cordner M. A., Smith K., Millar T. J., 2013, A&A, 550, A36
Millar, T. J., Walsh, C., Van de Sande, M., et al. 2024, A&A, 682, A109
Netzer, H.: AGN Emission Lines. In: Bladford, R.D., Netzer, H., Woltjer, L. (eds.) Active Galactic Nuclei, pp. 57–160. Saas-Fee Advanced Course of the Swiss Society for Astrophysics and Astronomy, Santa Fe (1990)
Peterson, B.M.: The Broad-Line Region in Active Galactic Nuclei. In: D., A., Johnson, R., Lira, P. (eds.) Physics of Active Galactic Nuclei at All Scales, 2006, vol. 693, pp. 77–100
Rokaki, E., Boisson, S., & Collin-Soufrin, S. 1992, A&A, 253, 57
Röllig, M., Abel, N. P., Bell, T., et al. 2007, A&A, 467, 187
Seyfert, C. 1948, ApJ, 97, 28
Shaw, G., Ferland, G. J., & Chatzikos, M. 2022, ApJ, 934, 53
Shaw, G., Ferland, G., & Chatzikos, M. 2023, Research Notes of the American Astronomical Society, 7, 153
Spyromilio, J. Meikle, W. P. S., Learner, R. C. M., & Allen, D. A. 1988, Nature, 334, 327
Tatulli, E., Malbet, F., Méniard, F., G. C., Testi, L., Natta, A., Kraus, S., Stee, P., & Robbe-Dubois, S. 2008, A&A, 489, 1151
Thomas, A. D., Groves, B. A., Sutherland, R. S., Dopita, M. A., Kewley, L. J. & Jin, C. 2016 ApJ, 833, 266
Thi, W.-F., Méniard, F., Meeus, G. et al. 2013, A&A, 557, A111
Thi, W.-F. & Bik, A. 2005, A&A, 438, 557
Thi, W.-F., van Dalen, B., Bik, A., & Waters, L. B. F. M. 2005, A&A, 430, L61
Thi, W. F., Hocuk, S., Kamp, I., et al. 2020, A&A, 634, A42

⁴ Slightly redshifted AGNs can be used to place such lines into much better atmospheric windows, without sacrificing too much in terms of the received flux.

Appendix A: Three-body reactions

At densities $> 10^{10} \text{ cm}^{-3}$, the rate of three-body reactions becomes competitive with two-body reactions. Three-body formation and destruction reactions of H_2 are accounted by default by the code. We complemented the reaction networks with three-body reactions taken from the UMIST2012 (McElroy et al. 2013).

Table A.1. Three-body (collider) reactions added to the standard CLOUDY network. The rate coefficients are taken from (McElroy et al. 2013). M designates H or H_2 .

Reaction		
$\text{CO} + \text{H} + \text{M}$	\rightarrow	$\text{O} + \text{C} + \text{H} + \text{M}$
$\text{CO} + \text{H}_2 + \text{M}$	\rightarrow	$\text{O} + \text{C} + \text{H}_2 + \text{M}$
$\text{CO} + \text{H} + \text{HOC}^+ + \text{M}$	\rightarrow	$\text{HCO}^+ + \text{CO} + \text{H} + \text{M}$
$\text{CO} + \text{H}_2 + \text{HOC}^+ + \text{M}$	\rightarrow	$\text{HCO}^+ + \text{CO} + \text{H}_2 + \text{M}$
$\text{C} + \text{O} + \text{H} + \text{M}$	\rightarrow	$\text{CO} + \text{H} + \text{M}$
$\text{C} + \text{O} + \text{H}_2 + \text{M}$	\rightarrow	$\text{CO} + \text{H}_2 + \text{M}$
$\text{H} + \text{O} + \text{H} + \text{M}$	\rightarrow	$\text{OH} + \text{H} + \text{M}$
$\text{H} + \text{O} + \text{H}_2 + \text{M}$	\rightarrow	$\text{OH} + \text{H}_2 + \text{M}$
$\text{H} + \text{OH} + \text{H} + \text{M}$	\rightarrow	$\text{H}_2\text{O} + \text{H} + \text{M}$
$\text{H} + \text{OH} + \text{H}_2 + \text{M}$	\rightarrow	$\text{H}_2\text{O} + \text{H}_2 + \text{M}$
$\text{H} + \text{CH}_3 + \text{H} + \text{M}$	\rightarrow	$\text{CH}_4 + \text{H} + \text{M}$
$\text{H} + \text{CH}_3 + \text{H}_2 + \text{M}$	\rightarrow	$\text{CH}_4 + \text{H}_2 + \text{M}$
$\text{H} + \text{NH}_2 + \text{H} + \text{M}$	\rightarrow	$\text{NH}_3 + \text{H} + \text{M}$
$\text{H} + \text{NH}_2 + \text{H}_2 + \text{M}$	\rightarrow	$\text{NH}_3 + \text{H}_2 + \text{M}$
$\text{H}_2 + \text{N} + \text{H} + \text{M}$	\rightarrow	$\text{NH}_2 + \text{H} + \text{M}$
$\text{H}_2 + \text{N} + \text{H}_2 + \text{M}$	\rightarrow	$\text{NH}_2 + \text{H}_2 + \text{M}$
$\text{O} + \text{O} + \text{H} + \text{M}$	\rightarrow	$\text{O}_2 + \text{H} + \text{M}$
$\text{O} + \text{O} + \text{H}_2 + \text{M}$	\rightarrow	$\text{O}_2 + \text{H}_2 + \text{M}$
$\text{H}_2 + \text{C} + \text{H} + \text{M}$	\rightarrow	$\text{CH}_2 + \text{H} + \text{M}$
$\text{H}_2 + \text{C} + \text{H}_2 + \text{M}$	\rightarrow	$\text{CH}_2 + \text{H}_2 + \text{M}$
$\text{H}_2 + \text{CH} + \text{H} + \text{M}$	\rightarrow	$\text{CH}_3 + \text{H} + \text{M}$
$\text{H}_2 + \text{CH} + \text{H}_2 + \text{M}$	\rightarrow	$\text{CH}_3 + \text{H}_2 + \text{M}$
$\text{C} + \text{N} + \text{H} + \text{M}$	\rightarrow	$\text{CN} + \text{H} + \text{M}$
$\text{C} + \text{N} + \text{H}_2 + \text{M}$	\rightarrow	$\text{CN} + \text{H}_2 + \text{M}$
$\text{C}^+ + \text{O} + \text{H} + \text{M}$	\rightarrow	$\text{CO}^+ + \text{H} + \text{M}$
$\text{C}^+ + \text{O} + \text{H}_2 + \text{M}$	\rightarrow	$\text{CO}^+ + \text{H}_2 + \text{M}$
$\text{C} + \text{O}^+ + \text{H} + \text{M}$	\rightarrow	$\text{CO}^+ + \text{H} + \text{M}$
$\text{C} + \text{O}^+ + \text{H}_2 + \text{M}$	\rightarrow	$\text{CO}^+ + \text{H}_2 + \text{M}$

Appendix B: Additional reaction

The reaction $\text{H} + \text{CO}$ has two branches: $\text{H} + \text{C} + \text{O}$ and $\text{C} + \text{OH}$. For completeness, we also added the reaction $\text{H} + \text{CO} \rightarrow \text{C} + \text{OH}$, which has an activation energy of 77700 K, to the CLOUDY network. In our models, the $\text{H} + \text{C} + \text{O}$ outcome dominates over the formation of OH.

Appendix C: Calcium chemistry

CLOUDY accounts by default for the ionization and recombination of atomic and ionized Ca. We complemented the default network with chemical reactions that includes Ca-bearing molecules. The reactions and rates are taken from the UMIST2022 network (Millar et al. 2024). The abundance for the Ca-bearing species for the two typical models are shown in Fig. C.1. The molecular Ca-species are at most two orders of magnitude less abundant than Ca or Ca^+ . In the high density model ($n_{\text{H}} = 10^{14} \text{ cm}^{-3}$), atomic Ca is the most abundance Ca-species so that the CaII lines probe only a fraction of the total neutral gas at high column densities.

Table C.1. Ca species reactions added to the standard CLOUDY network. The rate coefficients are taken from (Millar et al. 2024). Reactions with CRPHOT are Cosmic-Ray induced photoionization reactions and reactions with PHOTON are Far-UV photodissociation reactions.

Reaction		
$\text{Ca} + \text{CRPHOT}$	\rightarrow	$\text{Ca}^+ + \text{e}^-$
$\text{CaO} + \text{CRPHOT}$	\rightarrow	$\text{Ca} + \text{O}$
$\text{CaOH} + \text{CRPHOT}$	\rightarrow	$\text{Ca} + \text{OH}$
$\text{Ca} + \text{OH}$	\rightarrow	$\text{CaO} + \text{H}$
$\text{Ca} + \text{H}_2\text{O}$	\rightarrow	$\text{CaO} + \text{H}_2$
$\text{Ca} + \text{H}_2\text{O}$	\rightarrow	$\text{CaOH} + \text{H}$
$\text{Ca} + \text{CO}_2$	\rightarrow	$\text{CaO} + \text{CO}$
$\text{Ca} + \text{O}_2$	\rightarrow	$\text{CaO} + \text{O}$
$\text{CaO} + \text{H}$	\rightarrow	$\text{Ca} + \text{OH}$
$\text{CaO} + \text{H}_2$	\rightarrow	$\text{Ca} + \text{H}_2\text{O}$
$\text{CaO} + \text{O}$	\rightarrow	$\text{Ca} + \text{O}_2$
$\text{CaO} + \text{CO}$	\rightarrow	$\text{Ca} + \text{CO}_2$
$\text{CaOH} + \text{H}$	\rightarrow	$\text{Ca} + \text{H}_2\text{O}$
$\text{CaOH} + \text{H}$	\rightarrow	$\text{CaO} + \text{H}_2$
$\text{CaO} + \text{PHOTON}$	\rightarrow	$\text{Ca} + \text{O}$
$\text{CaOH} + \text{PHOTON}$	\rightarrow	$\text{Ca} + \text{OH}$

Appendix D: Photodissociation and self-shielding

Self-shielding against photodissociation for H_2 and CO are accounted for by the code as illustrated by Fig. D.1. In the figure, the photodissociation rates for H_2 and CO drop suddenly as soon as the relevant threshold column density is reached.

Appendix E: The BLR gas temperature profile

The gas temperature as function of depth for the 10^{12} and 10^{14} cm^{-3} models are shown in Fig. E.1 and Fig. E.2. The gas temperatures decrease with depth as photons are absorbed and cooler and molecular gas are more efficient gas coolants.

Appendix F: H_2 and CO main formation and destruction

Figure F.1 illustrates the main formation and destruction routes for H_2 and CO at steady-state for a model with density of 10^{12} cm^{-3} . The main reaction that actually forms H_2 from simpler H atoms is H_2 radiative recombination reaction. H_2 is destroyed at high column density by the formation of OH, which can react with C to form CO. OH is formed by the reaction $\text{O} + \text{H}_2$ with an activation barrier of $\sim 4000 \text{ K}$. This reaction is only relevant for gas hotter than $\sim 1000 \text{ K}$. The current network does not account for vibrational-excited H_2 reactions. OH can react with H to reform H_2 . At low column density CO is mostly destroyed by photodissociation. At column densities greater than 10^{26} cm^{-2} various reactions involving ions (N^+ , OH^+ , and He^+) contribute to CO destruction. A detailed discussion of the reaction paths can be found in Thi & Bik (2005). The H_2 formation via the radiative association $\text{H} + \text{H}$ is very low and its rate depends on the excitation state of H (Latter & Black 1991). In our models, the radiative association reaction is only important at very low column densities.

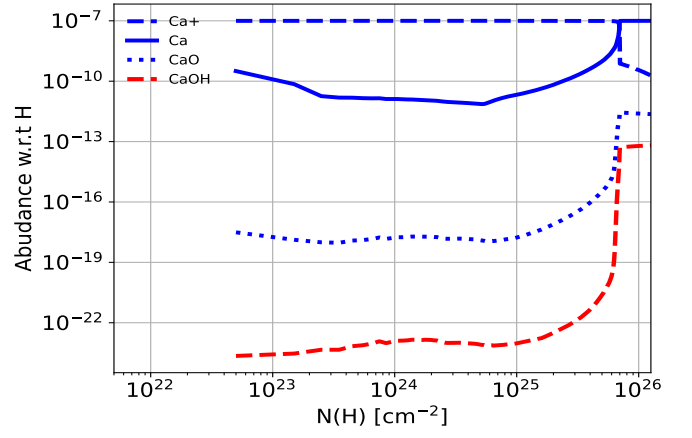
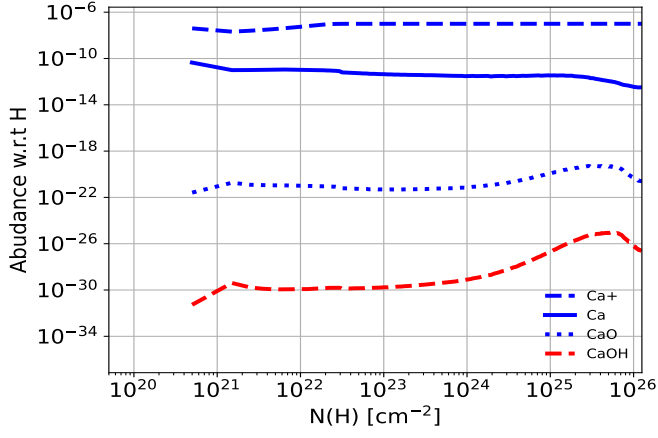


Fig. C.1. Abundance for Ca-bearing species as function of the column density, *Left*: A model with $n_{\text{H}} = 10^{12} \text{ cm}^{-3}$, $\log(U) = -3$, $\Delta V = 250 \text{ km s}^{-1}$, *Right*: A model with $n_{\text{H}} = 10^{14} \text{ cm}^{-3}$, $\log(U) = -5$, $\Delta V = 250 \text{ km s}^{-1}$.

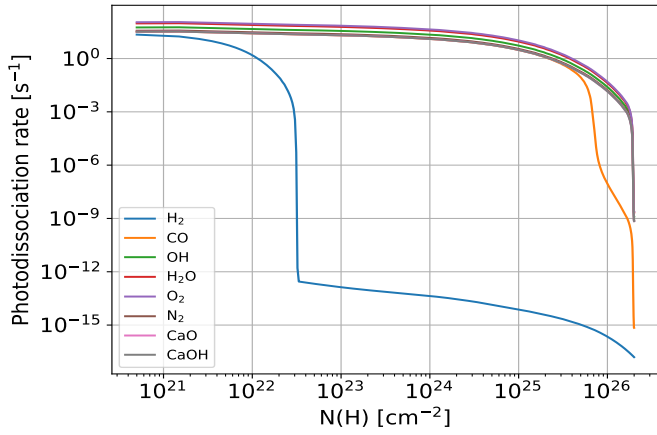


Fig. D.1. Gas temperature profile for a model with $n_{\text{H}} = 10^{12} \text{ cm}^{-3}$, $\log(U) = -3$, $\Delta V = 250 \text{ km s}^{-1}$.

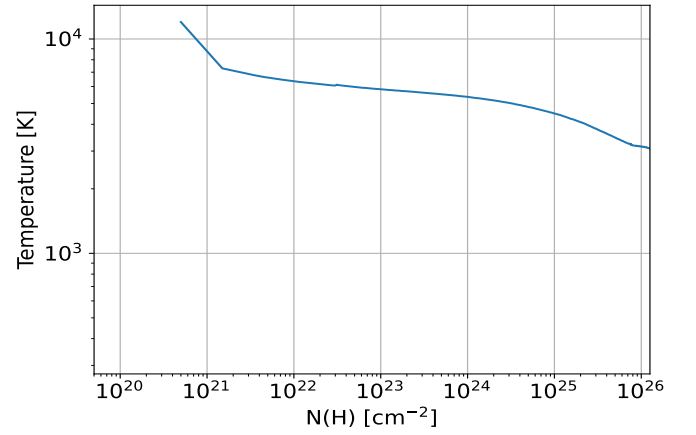


Fig. E.1. Gas temperature profile for a model with $n_{\text{H}} = 10^{12} \text{ cm}^{-3}$, $\log(U) = -3$, $\Delta V = 250 \text{ km s}^{-1}$.

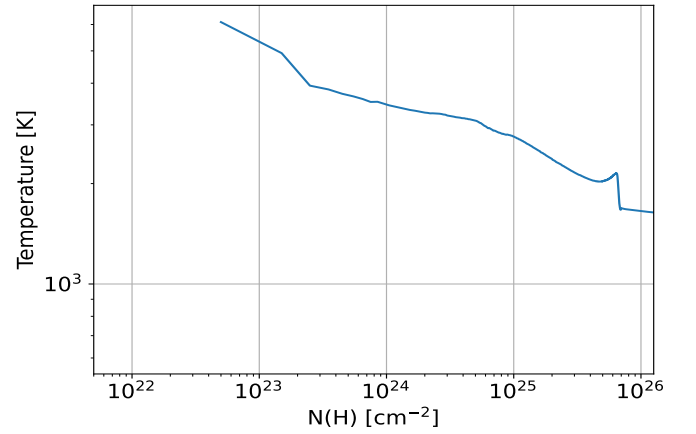


Fig. E.2. Gas temperature profile for a model with $n_{\text{H}} = 10^{14} \text{ cm}^{-3}$, $\log(U) = -5$, $\Delta V = 250 \text{ km s}^{-1}$.

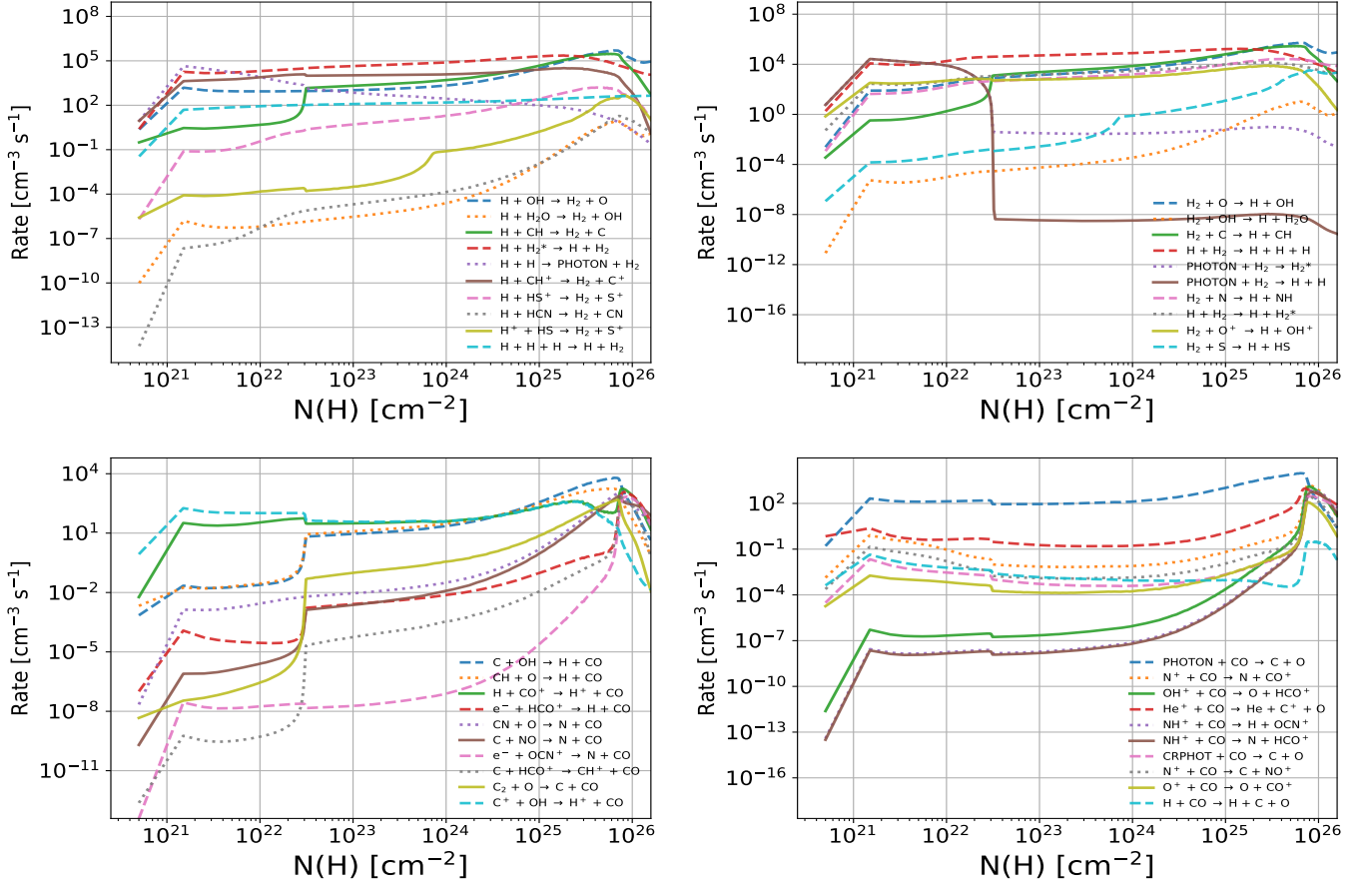


Fig. F.1. Main formation (left panels) and destruction (right panels) reactions for H_2 and CO for the $n_{\text{H}} = 10^{12} \text{ cm}^{-3}$, $\log(U) = -3$, $\Delta V = 250 \text{ km s}^{-1}$ model. Only the top 10 main formation and destruction reactions are shown